JACS
JOURNAL OF THE AMERICAN CHEMICAL SOCIETY

Article

pubs.acs.org/JACS

Amphiphilic Perylene–Calix[4]arene Hybrids: Synthesis and Tunable Self-Assembly

Fabian Rodler,[§] Boris Schade,[‡] Christof M Jäger,[¤,†] Susanne Backes,[§] Frank Hampel,[§] Christoph Böttcher,*[,‡] Timothy Clark,[†] and Andreas Hirsch*[,§]

[§]Department of Chemistry and Pharmacy, Interdisciplinary Center of Molecular Materials (ICMM), Friedrich-Alexander-University of Erlangen-Nürnberg, Henkestrasse 42, 91054 Erlangen, Germany

[‡]Research Center for Electron Microscopy, Department of Chemistry and Biochemistry, Freie Universität Berlin, Fabeckstrasse 36a, 14195 Berlin, Germany

[¤]Department of Chemical and Environmental Engineering, University of Nottingham, University Park, Nottingham NG7 2RD, United Kingdom

[†]Computer-Chemie-Centrum and Interdisciplinary Center of Molecular Materials, Department of Chemistry and Pharmacy, Friedrich-Alexander-University of Erlangen-Nuremberg, Nägelsbachstrasse 25, 91052 Erlangen, Germany

Supporting Information

ABSTRACT: The first highly water-soluble perylene–calix[4]arene hybrid with the calixarene scaffold acting as a structure-determining central platform is presented. In this tetrahedrally shaped amphiphilic architecture the hydrophilic and hydrophobic subunits are oriented at the opposite side of the calixarene platform. The hydrophobic part contains the two perylene diimide moieties, which enable strong $\pi-\pi$ interactions in self-assembly processes. Two hydrophilic Newkome-type dendrons provide sufficient water solubility at slightly basic conditions. The tetrahedrally shaped amphiphile displays an unprecedented aggregation behavior down to concentrations as low as 10^{-7} mol L^{-1}. The intriguing self-assembly process of the compound in water as well as under changed polarity conditions, achieved by addition of THF, could be monitored by the complemented use of cryogenic transmission electron microscopy (cryo-TEM), UV–vis spectroscopy, and fluorescence spectroscopy. Molecular-dynamics and molecular modeling simulations helped in understanding the interplay of supramolecular and optical behavior.

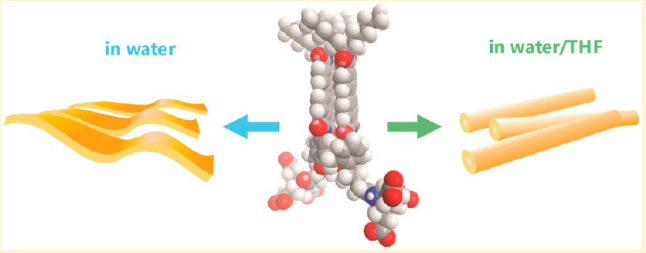

INTRODUCTION

Self-assembly of amphiphilic molecules in aqueous media is a fundamental process not only in nature but also in supramolecular chemistry.[1,2] Shape, size, and intermolecular interactions of the individual building blocks are important factors which drive the self-assembly process toward their three-dimensional supramolecular architecture.[3] Despite many efforts, the prediction (hierarchical structure, shape, size, stability, uniformity) of nanoarchitectures represents still a very challenging and unsolved task.[4] Among synthetic amphiphiles calixarene derivatives have recently attracted increasing attention.[5] This is in particular due to the quite rigid and bowl-shaped calixarene scaffold which can easily be chemically modified both at the upper and the lower rim. Recently, we reported on the first appearance of shape persistent micelles composed of dendro-calix[4]arenes **1** and **2**,[6,7] whose supramolecular structures were determined by pulse field gradient spin–echo NMR spectroscopy (PGSE-NMR) and cryogenic transmission electron microscopy (cryo-TEM). Because of the shape persistence of the assembly structures a reconstruction of their three-dimensional structure was possible allowing for the exact allocation of individual molecules within the assemblies. In the case of dendro-calix[4]arene **2**, additional specific counterion effects were observed, directing stabilization by sodium rather than potassium counterions.[8,9] Accompanying MD calculations revealed the preference of sodium ions for ion pairing with carboxylates which reduces electrostatic repulsions of the charged head groups.

With regard to their photostability and characteristic UV–vis absorption properties, perylene diimide dyes play an important role in supramolecular dye chemistry as highly potent fluorescent sensors as well as n-type semiconductors[10,11] or extended exciton mobility materials.[12] These optical and electronic properties are caused by local $\pi-\pi$ stacking interactions of the perylenes skeletal structure leading to H or J aggregated nanostructures.[13] The electronic and photochemical properties of selectively trans-substituted perylene–calix[4]arene conjugates were studied in a couple of reports.[14,15] Therein, remarkably efficient energy transfer

Received: December 1, 2014
Published: February 19, 2015

DOI: 10.1021/ja512048t
J. Am. Chem. Soc. 2015, 137, 3308–3317

processes of light harvesting of up to five perylene diimide units connected by calix[4]arenes were reported.[14]

Herein, we report on the synthesis and the aggregation behavior of a new prototype of amphiphile, namely a tetrahedrally amphiphilic substituted calix[4]arene with an opposite arrangement of the hydrophilic and hydrophobic building blocks at the upper and the lower rim of the calixarene platform. The construction principle contrasts that of the compounds **1** and **2** (Scheme 1) inasmuch as the tetrahedral

Scheme 1

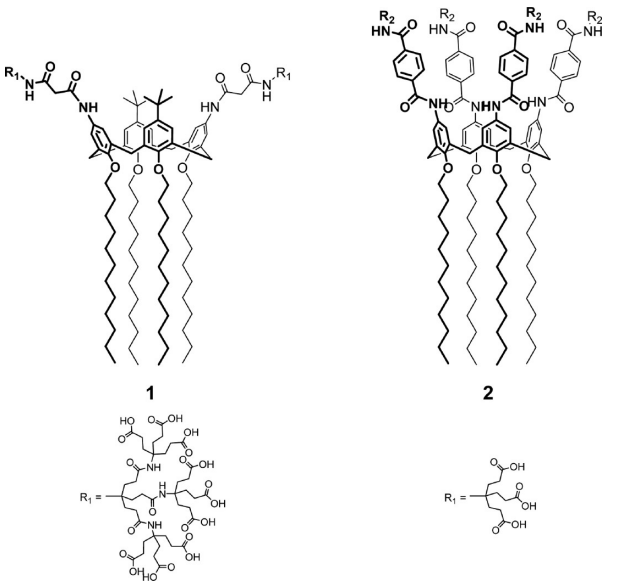

architecture of the bis-peryleno bis-dendro calix[4]arene (**PDC**, **3**) is based on a trans−trans substituted calixarene cage and was designed to allow for the adoption of two different so-called *pinched-cone* conformations[16] to regulate the self-assembly process in a directed fashion. The lower rim of the calixarene core was substituted with two Newkome-type first generation dendrons (G1) to provide proper water solubility. The upper rim was selectively trans-functionalized with two perylene diimide moieties in the 5,17-position (Figure 1A), where large aromatic scaffolds allow for favorable $\pi-\pi$ stacking interactions which in turn can be used to monitor the aggregation process with spectroscopic methods. As a positive side effect, the introduction of such large aromatic systems enables high electron contrast in cryo-TEM images. The absence of substituents in the 11,23 position (upper rim) and in 26,28 position (lower rim) of the calix[4]arene scaffold further allows for pronounced angle broadening, which is a prerequisite for adopting the depicted tetrahedral structure (open conformation in Figure 1B) based on one of the pinched-cone conformations of the calixarene. Our cryo-TEM data as well as corroborating molecular dynamics (MD) simulations, however, show that a transformation into the closed conformation (Figure 1C) can be triggered by hydrophobic and $\pi-\pi$ stacking interactions. This is in line with an observation of Würthner et al. reporting on the interconversion equilibrium between the open and closed pinched-cone conformations in a series of lipophilic calix[4]arenes.[17]

We will also show that a remarkably uniform aggregation mode of **PDC** can be stimulated by changing the solvent polarity. Cryo-TEM data exhibit the formation of uniform fibrous micelles if using a binary mixture of water and THF as the solvent. Simultaneously, this gives way to the formation of highly ordered structures (extended lamellae and nanocrystalline platelets) before eventual precipitation of microcrystalline **PDC** occurs.

METHODS

Concept of Synthesis. The targeted substitution pattern of **PDC** (Figure 1) required to develop a very selective reaction sequence in order to provide efficient access to this new compound type (Scheme 1). Especially, during the first steps, where the bulky substituents at the hydroxyl groups are still missing, the complete conformational flexibility of the basic calix[4]arene **4** reflects a considerable obstacle. For example, during the nitration reaction of the intermediate **6**, not only appropriate stoichiometric equivalents of the reactants but also the correct synthetic succession is of crucial importance to achieve desired 5,17- and 25,27-substitution at the calix[4]arene cage. In the end, **PDC** was obtained by the six step synthesis depicted in Scheme 2 with an overall yield of 16%.

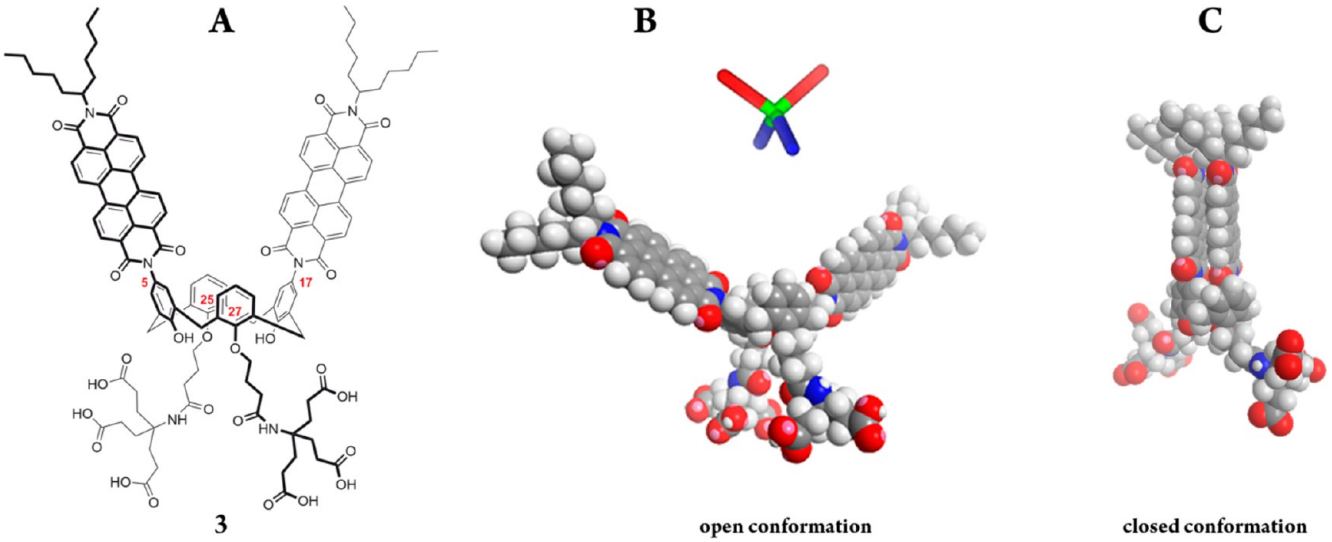

Figure 1. (A) Lewis-structure of bis-peryleno bis-dendro calix[4]arene (**PDC**, **3**). (B,C) CPK-models of conformation of **PDC**: (B) open conformation, (C) closed conformation. The tetrahedral scheme (middle) displays the allocation of hydrophobic (red) and hydrophilic parts (blue).

DOI: 10.1021/ja512048t
J. Am. Chem. Soc. 2015, 137, 3308−3317

Scheme 2[a]

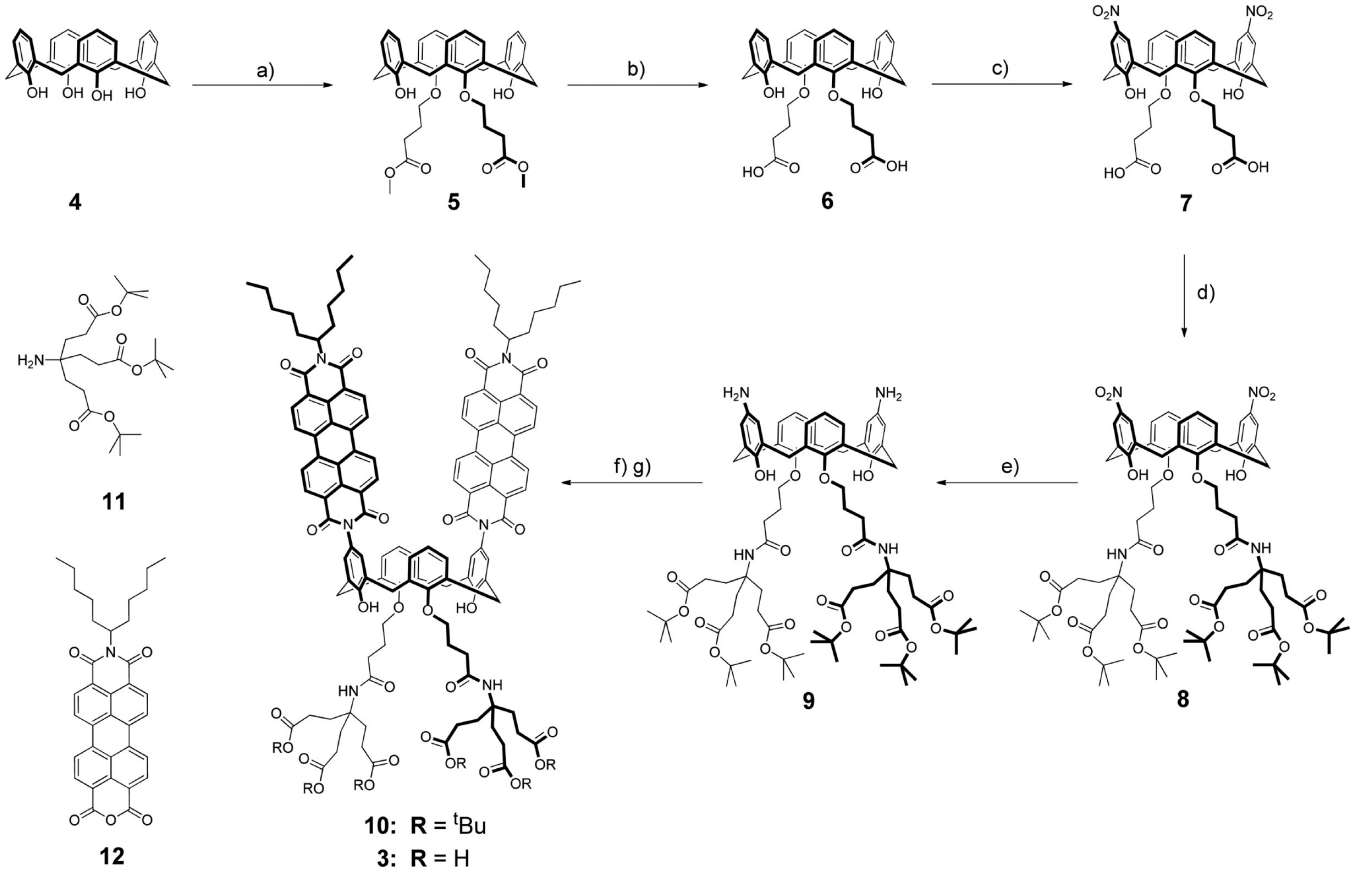

[a]Synthesis of the perylene derived dendro-calix[4]arene **10**. Reagents and conditions: (a) methyl 4-bromobutyrate, K_2CO_3, acetonitrile 80 °C, 12 h; (b) KOH, acetone, room temperature, 4d; (c) HNO_3 (65%), AcOH (100%), CH_2Cl_2, 0 °C, 15 min; (d) H_2N-G1-^{t}Bu (**11**), DMT-MM, THF, room temperature, 4 h; (e) Pd/C, N_2H_4*H_2O, EtOH, 90 °C, 12h; (f) **12**, zinc acetate, quinoline, 120 °C, 2 h; (g) $CHCl_3$, formic acid.

The starting material 25,26,27,28-tetrahydroxy-calix[4]arene **4** was synthesized as described in the literature.[18] The reaction of **4** with 4 equiv of methyl 4-bromobutyrate and 2 equiv of potassium carbonate afforded a mixture of four possible alkylation products, which have to be separated by slow recrystallization from methylene chloride/methanol to finally obtain 25,27-dialkoxy-26,28-dihydroxy-calix[4]-arene **5** in 77% yield. Because of strong hydrogen-bonding interactions of the hydroxyl groups at the lower rim the flexibility of the calix[4]arene cage is considerably reduced in aprotic solvents like methylene chloride. Single crystals of **5** could be obtained (see Supporting Information V). X-ray analysis reveals a triclinic arrangement (space group P-1) where the elementary cell consists of two antiparallel orientated molecules. After hydrolyzing the methyl ester groups with potassium hydroxide in acetone at room temperature, 5,17-dinitrocalix[4]arene-dicarboxylic acid **7** was obtained by electrophilic aromatic nitration at the 5,17-positions of the calix[4]arene in 62% yield. The pronounced regioselectivity during the formation of **7** was provided by the strong mesomeric effect of the hydroxyl groups. Furthermore, the exact reaction time as well as controlled temperature conditions has to be maintained to promote the preferred formation of the 5,17-substituted nitro compound **7** and prevent the formation of mono-, di(5,11), tri-, and tetra-substituted derivatives. In the next step, the butyric acid substituents of **7** were coupled with the first generation Newkome Dendron **11** (H_2N-G1-*t*Bu[19]) in a 4-(4,6-dimethoxy-1,3,5-triazin-2-yl)-4-methylmorpholinium chloride (DMT-MM) assisted aminolysis reaction before the nitro groups were reduced with hydrazine−monohydrate by palladium-catalyzed hydrogenolysis. The resulting highly oxidation-sensitive diamino-calix[4]-arene **9** was condensed with perylene monoimide−monoanhydride **12**[20] in quinoline under inert conditions before, finally, the *tert*-butyl esters were cleaved with formic acid in $CHCl_3$ at room temperature. All compounds were characterized by NMR- and IR-spectroscopy, mass-spectrometry and in part by elemental analysis; compounds **10** and **3** were additionally characterized by UV−vis and fluorescence spectroscopy. (Detailed information on the synthetic procedures and structural analysis of all new compounds are given in the Supporting Information).

PDC is completely insoluble both in nonpolar as well as in polar solvents. Even in water it dissolves only at higher pH values (>8.5). However, the octa-sodium or -potassium salts (**PDC**$^{8-}$) are readily soluble in pure water at moderate concentrations up to 10^{-2} mol L^{-1}. During the dissolution of these salts the pH values become highly basic caused by the instantaneous protonation of the sodium phenolate groups. Unless otherwise noted, sample solutions used for UV−vis and fluorescence spectroscopy as well as for cryo-TEM-measurements were prepared from the **PDC**$^{8-}$ octa alkali salts.

UV−Visible Measurements. Absorption spectra were measured with either a Cary 5000 UV−vis−NIR spectrometer or a Cary 50 spectrophotometer (Varian Inc., Australia) using quartz cuvettes (Hellma, Germany). The Cary 50 instrument is equipped with a temperature-controllable multicell holder.

Fluorescence Measurements. Emission spectra were measured with a RF-5301 PC spectrofluorophotometer (Shimadzu, Japan) using quartz cuvettes (Hellma, Germany). Excitation wavelengths are specified in the corresponding figure caption.

Cryogenic Transmission Electron Microscopy. Samples for cryo-TEM investigations were prepared according to our standard method (see Supporting Information). Microscopy was conducted using a Philips CM12 (100 kV, LaB_6-illumination) at a primary magnification of 58300×. CM12 data were recorded on Kodak

DOI: 10.1021/ja512048t
J. Am. Chem. Soc. 2015, 137, 3308−3317

electron image film SO-163 (Eastman Kodak Company, USA) and digitized for image processing to a final pixel resolution of 0.686 Å/pixel.

Molecular Modeling. Atomistic Molecular Dynamics (MD) simulations were performed using the Amber 12 suite of programs.[21] The force field parameters for **PDC** are based on the General Amber Force Field (GAFF)[22] together with atomic charges derived using the restrained electrostatic potential (RESP) fitting procedure by Kollman et al.[23] and on special adjustments outlined in the Supporting Information. Monomers of **PDC** were simulated for at least 100 ns simulation time; the formation of dimers and trimers was observed in simulations of six monomers for simulation times up to 250 ns. Details for the simulation protocols can be found in the Supporting Information.

Umbrella sampling (US) simulations followed by the weighted histogram analysis method (WHAM)[24] were used to calculate the relative free energy differences between the open and the closed conformation of the **PDC** monomers.

CPK models were created using the Chem3D Pro 14 software (CambridgeSoft Corporation, PerkinElmer, USA).

RESULTS AND DISCUSSION

The aggregation behavior of **PDC** in water and in binary water/THF mixtures at different THF content was monitored by means of the electronic properties of the perylene diimide moieties by the use of UV−vis and fluorescence spectroscopy as well as regarding the supramolecular organization using cryogenic transmission electron microscopy (cryo-TEM). Interpretation of the results was assisted by MD calculations and molecular modeling.

Spectroscopic Properties of PDC in $CHCl_3$/TFA. The UV spectrum of the free acid of **PDC** in $CHCl_3$/TFA (9:1, Figure 2 red line) at a concentration of 1.0×10^{-5} mol L^{-1}

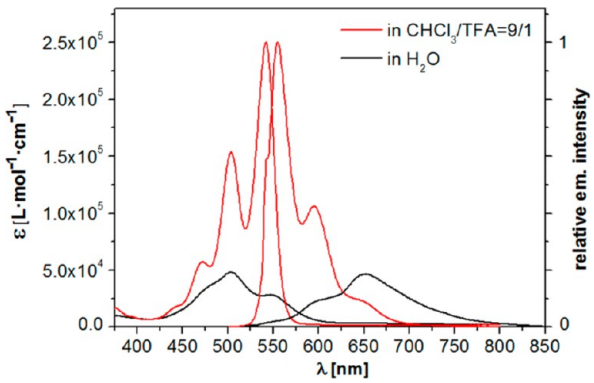

Figure 2. UV−vis absorption and emission spectra of **PDC** in water and the completely protonated **PDC** in CHCl3/TFA (9/1), respectively: red line, absorption and emission spectra in CHCl3/TFA, 1.0×10^{-5} M; black line, absorption and emission spectra in water, 5.0×10^{-5} M. Excitation wavelength: in $CHCl_3$/TFA, 540 nm; in H2O, 491 nm.

exhibits the well-resolved vibronic structure of three bands at 472, 504, and 542 nm with increasing intensity representing the 2−0, 1−0, and 0−0 transition (designation of the transitions was carried out according to Spano et al.[25]), respectively, of the S_0−S_1 band of the perylene chromophore polarized along the long molecular axis.[26] The absorption coefficient (ε) of the most intensive band (λ_{max}) at 542 nm amounts to 2.50×10^5 L^{-1} mol^{-1} cm^{-1}, which is about more than double the typical values of nonpolar perylene conjugated calix[4]arenes investigated in aprotic solvents by Würthner et al.[17] In our case, both the shift of λ_{max} and the large ε-value may arise from the stabilization of the charge separated excited state in the highly polar solvent and from the increased electron density of the perylene units due to the strong +M-effect of the hydroxyl groups in the para position.

The fluorescence spectrum of **PDC** in $CHCl_3$/TFA (Figure 2, red line) is slightly Stokes-shifted by about 13 nm (432 cm^{-1}, 54 meV) and displays three bands at 555, 595, and 647 nm with intensity ratios comparable to the UV−vis bands but in reversed order. The overall shape of both UV−vis and fluorescence spectra, with the 0−0 transition being the strongest, is characteristic for non-π-stacked (nonaggregated) perylene diimides.[27,28]

Aggregation Behavior in Water. Compared to the spectroscopic characteristics of completely protonated **PDC** in $CHCl_3$/TFA, pronounced changes of the absorption and emission features (Figure 2, black lines) occur in water. Here, the UV−vis spectrum displays three bands at 477, 503, and 547 nm with considerably decreased overall absorption (approximately 1 order of magnitude) and interchanged intensity ratios, that is, the second band, representing the 1−0 transition, becomes the most intensive band ($\varepsilon = 4.80 \times 10^4$ L^{-1} mol^{-1} cm^{-1}). The fluorescence spectrum displays broadened transitions at 601 and 652 nm of mirrored intensities (compared to the UV−vis bands) with a large Stokes-shift of 56 nm (1698 cm^{-1}, 211 meV). The overall emission is decreased to about 20% compared to the spectrum recorded in $CHCl_3$/TFA. The specified spectral changes are characteristic for the H-type aggregation of perylene bisimides.[10]

Concentration dependent UV−vis studies of **PDC** in water in the range of 10^{-2} mol L^{-1} to 10^{-7} mol L^{-1} showed neither a shift of the absorption maxima nor a change of the signal intensity ratios ($I_A{}^{0-0}/I_A{}^{1-0} = 0.6$) over the entire concentration range (Supporting Information, Figure SI 15) . This indicates an almost exclusive occurrence of perfectly cofacial stacked perylenes even at the very low concentration of 10^{-7} mol L^{-1} and thus, points to intramolecular π interactions rather than intermolecular ones.

In the fluorescence spectra, the picture is slightly different (Figure 3A). Starting at a concentration of 10^{-4} mol L^{-1}, a broad emission with a maximum at 652 nm and a shoulder around 600 nm indicates the exclusive presence of aggregated perylenes. By dilution to 5.0×10^{-5} mol L^{-1}, however, two new peaks appear at 555 and 737 nm (a small shoulder for the latter peak is only visible in the original spectrum), respectively. The origin of the long-wave emission is not known, its band intensity declines gradually with decreasing concentration of **PDC**. In contrast, the intensity of the additional short-wave emission at 555 nm initially rises upon dilution and only falls off beyond a PDC concentration of 10^{-5} mol L^{-1} (red curve in Figure 3B). According to Würthner et al.,[17] this band must be attributed to the 0−0-transition of free perylene diimide moieties of monomers. Since this transition is only allowed for nonaggregated perylenes and concerns the strong fluorescence quenching in aggregates (cp. fluorescence in binary water/THF mixtures), this band is extremely sensitive to the occurrence of monomeric perylenes and hence indicative as to the CMC of the aggregation process of **PDC**. Their number, however, must be very small, evidenced by the strong fluorescence quenching in aggregates (cp. fluorescence in binary water/THF mixtures)

To obtain direct structural data of **PDC** in water cryo-TEM investigations were carried out, which initially revealed a high structural polydispersity. A variety of twisted and curved ribbon-like structures of different width were found in the 1

DOI: 10.1021/ja512048t
J. Am. Chem. Soc. 2015, 137, 3308−3317

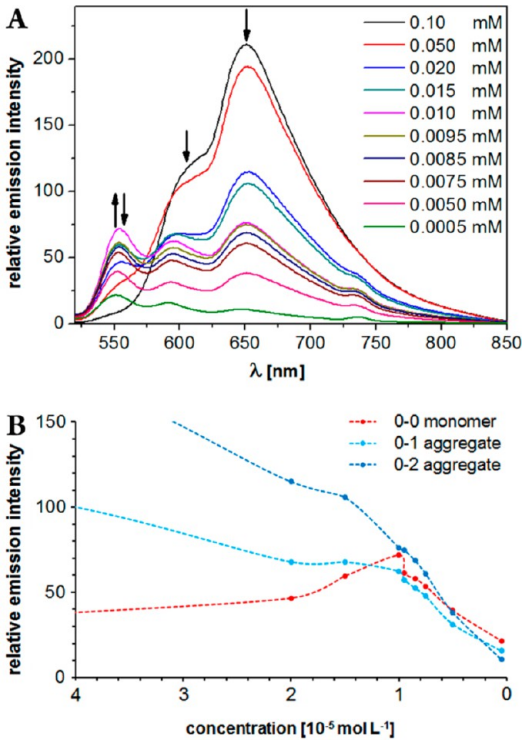

Figure 3. (A) Fluorescence spectra of a dilution series of **PDC** in water reflect a deaggregation process around 10^{-5} mol L^{-1} which is indicated by the abrupt rise of a 0−0 emission peak at 555 nm indicative for monomeric perylene diimides. (B) The intensity course of this peak reveals a sudden increase of the number of free perylene moieties and a congruent decrease with the emissions rate of the aggregated species (blue lines) upon further dilution. Excitation wavelength: 491 nm.

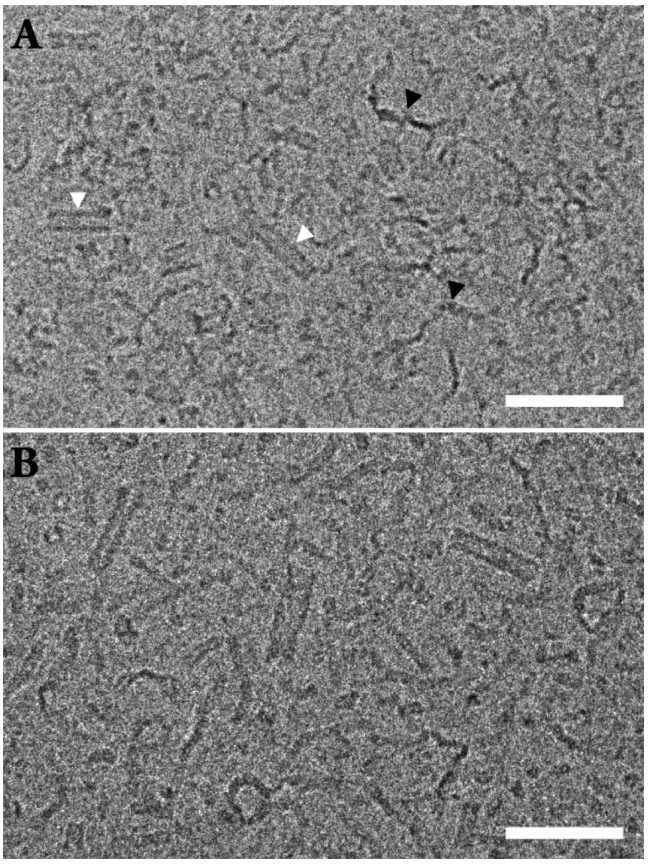

Figure 4. Cryo-TEM images of a 1.0 mM solution of **PDC** in water. (A) Tubular aggregates (white arrowheads) and ribbon-like assemblies (black arrowheads) are the predominant assembly structures. (B) After 5 h's of annealing at 85 °C the polymorphous appearance of the sample prevails. Bars indicate 50 nm.

mM solution (Figure 4A, black arrowheads). Since these ribbons adopt different orientations in the vitrified layer their thickness can be deduced from side view projections to be 1.8 to 2.5 nm.

In addition, short tube-like aggregates can be observed (Figure 4A, white arrowheads), which appear to be rigid with diameters between 8−20 nm and lengths ranging from 8 up to 100 nm. The tubes exhibit a uniform wall thickness of 1.8−2.5 nm and thus correspond to the thickness of the accompanying ribbons. There are numerous examples in the literature that illustrate the close relationship between twisted micellar ribbons and tubes.[29] The theoretical framework for the structural correlation between these aggregation modes was provided by Helfrich only in 1986.[30] Therefore, it is reasonable to assume that both types of aggregates are based on the same molecular construction principles.

The polymorphous appearance of the samples, however, suggests a kinetically rather than a thermodynamically driven aggregation process, that is, the sample seems to clearly diverge from being at a thermodynamical equilibrium. We therefore tried to bias the aggregation at elevated temperatures in order to obtain more uniform aggregates.

However, annealing the aqueous solution for 5 h at 85 °C and slow cooling did not change the heterogeneous appearance of the aggregates (Figure 4B) indicating thermal stability of the aggregates in this temperature range. This is confirmed by UV−vis spectra which showed only a negligible shift of 3 nm and small changes in the intensity ratios from 1.43 to 1.37 (1−0 transition to 0−0 transition) over the entire temperature range of 25 °C up to 85 °C. Both small changes reversed upon cooling (Supporting Information, Figure SI 17).

Aggregation Behavior in Binary Water/THF Mixtures. The polarity of water is gradually changed by the addition of THF.[31] Inspired by a recent report of Rybtchinsky et al.,[32] we investigated the influence of the solvent polarity on the aggregation behavior of the **PDC** using different mixtures of water with THF. Thereby, two different preparation pathways were operated. In the "dilution method" we added specific amounts of THF to a pure aqueous stock solution of **PDC**, while in the "direct method" we dissolved **PDC** salt directly in respective binary water/THF mixtures. All samples were kept properly sealed to avoid unwanted evaporation of THF during the observation period.

Dilution Method. By adding increasing amounts of THF to a 0.1 mM aqueous stock solution the absorption spectra considerably changed (Figure 5). Starting from pure water, the 0−0 transition and 1−0 transition are both hypsochromically shifted from 547 to 529 nm ($\Delta\lambda$ = 18 nm) and from 503 to 497 nm ($\Delta\lambda$ = 6 nm) up to a ratio of 30% THF (v/v). A further increase of the THF ratio causes a steep ascent of the molar absorption and the hypsochromical shift of the 1−0 band continues to 489 nm ($\Delta\lambda$ = 8 nm). Both are accompanied by an inversion of the band intensities (I_A^{0-0}/I_A^{1-0} changes from 0.6 in pure water to 1.45 at 75% THF); that is, the 0−0 transition now becomes the most intensive, indicating the ongoing decrease of π stacking interactions between the PDI

DOI: 10.1021/ja512048t
J. Am. Chem. Soc. 2015, 137, 3308−3317

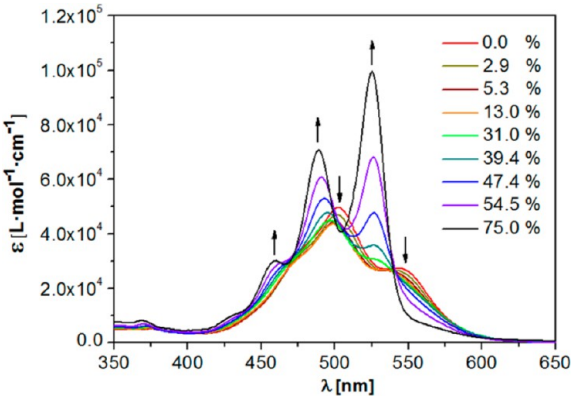

Figure 5. UV−vis spectra of the titration of a 0.1 mM stock solution of **PDC** in water with THF (the THF content is given in volume percent). The dilution during titration effected a final concentration of 2.5×10^{-5} mol L^{-1} of **PDC** at 75% THF.

moieties. Accordingly, with increasing amounts of THF the solution color changes from deep red (in pure water) to a strongly fluorescent orange. Finally, at a THF ratio of 75%, the complete spectrum is hypsochromically shifted about 22 nm (766 cm^{-1}, 95 meV) according to the change in the solvents polarity. Comparable shifts for substituted perylene bisimides[28,33] and for PDI-calix[4]arene derivatives were reported by Würthner et al.[17,27]

The UV−vis results were supported by corresponding fluorescence measurements (cp. Supporting Information, Figure SI 16). At the outset (in pure water) the spectrum displays three emission maxima at 555, 595, and 652 nm with mirror like intensities compared to the UV−vis spectrum of the pure aqueous solution (Figure 2). The band intensities gradually equal and shift toward lower wavelengths upon addition of THF until at a critical ratio between 33% and 37% THF the emission maxima became inversed, that is, the band at 548 nm becomes the most intensive one. At the same time, the emission intensity increases (by a factor of about 20) and the whole fluorescence spectrum is hypsochromically shifted ($\Delta\lambda$ = 16 nm, 462 cm^{-1}, 57 meV). The steep increase in intensity conversely indicates a strongly quenched fluorescence of the aggregates if compared to the free perylene moiety.

The shift of the relative band intensities in UV−vis and fluorescence spectra indicates the gradual decrease of the perylene $\pi-\pi$ interactions in response to the lowering of the solvent polarity. Noteworthy, at a THF ratio of 90%, **PDC** precipitates as an orange colored solid within 1 day.

Complementing the spectral changes on a supramolecular level, we performed cryo-TEM measurements of a 0.95 mM (5% THF) and a 0.70 mM (30% THF) sample, both prepared from a 1 mM aqueous stock solution of **PDC**. As was expected from the spectra, in the presence of only 5% THF no changes occurred even after 5 weeks. By the addition of 30% THF, however, the formation of uniform fibrous aggregates of several hundred nanometers in length and 4.5−5.6 nm in diameter could be observed (Figure 6A). After 1 week these aggregates proliferate into a dense network which completely occupies the vitrified sample layer (Figure 6B). After 5 weeks, their number was significantly decreased while their diameters were slightly increased to ∼6−7 nm. Instead regular striations with a repetitive distance of 3.4 ± 0.4 nm prevail (Figure 6C). These striations are reminiscent of a liquid crystalline lamellar phase and probably indicate a preliminary stage of the macroscopically observed precipitation (crystal formation), which eventually occurred in all binary water/THF mixtures even at the lowest concentrations of 10^{-7} mol L^{-1}.

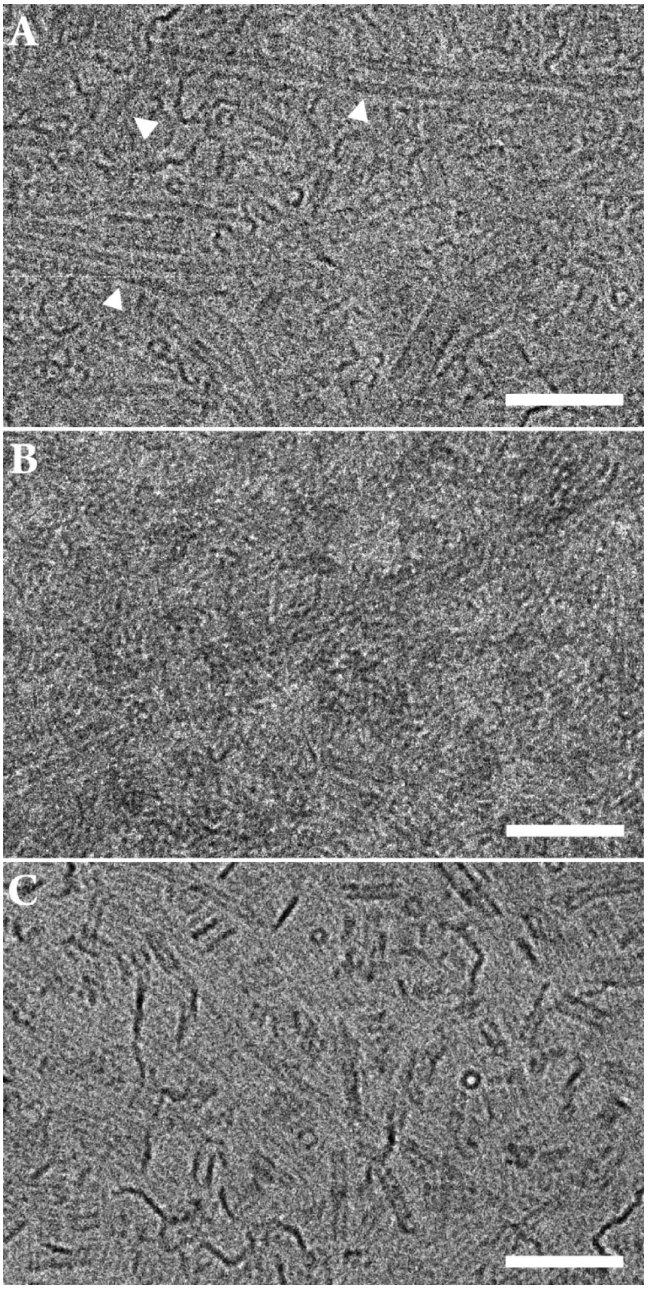

Figure 6. Progress of the aggregation process of **PDC** (0.7 mM) in a binary water/THF mixture (70:30, v/v, dilution method) can be visualized by cryo-TEM. (A) Immediately after THF admixing, next to the polymorphous waterborne structures, the formation of fibrous aggregates (white arrowheads) of 4.5−5.6 nm in diameter and lengths of several hundred nanometers can be observed. (B) A dense network of these fibrous aggregates has formed within 1 week. (C) After 4 weeks, however, the fibrous aggregates have almost disappeared. Instead, regular striations of 3.4 nm line width overlie the images, which still show ribbons and tubes. Bars indicate 50 nm.

Interestingly, despite changes in the structure, an additional almost invariant background of ribbons and tubes is detected which most probably remained from the pristine aqueous stock solution (*vide supra*). These ribbons and tubes are obviously stable even under the changed polarity conditions. This is

DOI: 10.1021/ja512048t
J. Am. Chem. Soc. 2015, 137, 3308−3317

corroborated by our findings that such waterborne aggregates are completely absent, if **PDC** is directly dissolved in water/THF.

Direct Method. The above-described aggregation progress is markedly accelerated if the **PDC** salt is directly dissolved in the respective binary water/THF mixture (1 mM, 30% THF). In this case, the dense network of only fibrous aggregates is formed immediately after dissolution. After 6 days, the number of the fibrous assemblies has decreased, so that individual aggregates and small circular structures of high contrast, thought to represent top views of shorter fibers, are now observed (Figure 7A). Image analysis (see Supporting Information section III.b) of the fibrous aggregates revealed an increase of the mean fiber diameter from 5.45 to 7.63 nm within these first 6 days. Thereby, the thickness of the "walls" did not notably change. The indicated swelling process seems to be completed within this first week (no further change of the aggregate diameter can be observed after 26 days).

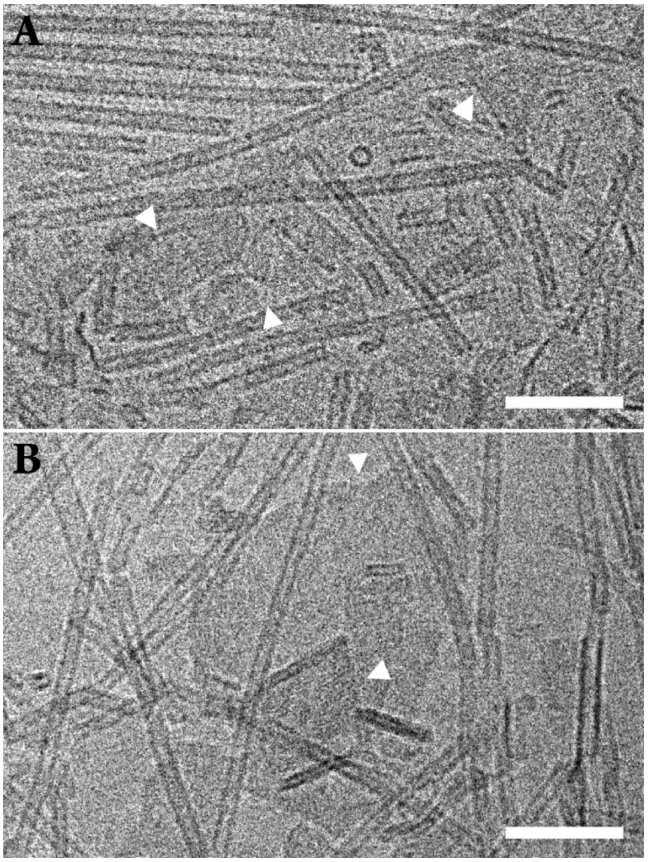

Figure 7. When **PDC** was directly dissolved in the water/THF mixture (70:30, v/v) a dense population of fibrous aggregates was immediately formed. (A) After 6 days the number of aggregates is drastically reduced; 3.6 nm striations (cp. Figure 6C) and small platelets (white arrowheads) are present at this stage of the aggregation process. (B) After 26 days the number of fibrous aggregates is further reduced and the 3.6 nm striation has completely disappeared. Instead, platelets have now grown larger and can display 1.9 nm lattice layer spacings (cp. Supporting Information, Figure SI 19). Bars indicate 50 nm.

Direct dissolution of the **PDC** salt in the binary water/THF mixture also accelerates the formation of periodical striations, and areas with line spacings of 3.6 ± 0.4 nm are detectable already 6 days after preparation. Also smaller platelets appear, which might indicate the nanoscopic evidence for a beginning crystallization process, which is eventually macroscopically evidenced by precipitation of orange colored crystals.

After 26 days, most of the fibrous aggregates vanished. Now more structurally defined crystal patches occur showing 1.95 nm lattice layer spacings (Figure 7B and Supporting Information, Figure SI 19).

This time dependent evolution of the aggregation behavior of the PDC in water/THF is not reflected by corresponding changes of the UV−vis spectra. Nevertheless, the absorption intensity decreases already after 1 week, and therefore, precedes the visible crystal precipitation which happens only after 18 days. As mentioned above, this precipitation occurs even from highly diluted solutions with concentration as low as 10^{-7} mol L^{-1}.

UV−vis studies of serial dilutions of **PDC** directly dissolved in water/THF (70:30, v/v) were performed at concentrations ranging from 10^{-2} mol L^{-1} to 2.5×10^{-5} mol L^{-1} (Figure 4). For high concentrations (10^{-2} mol L^{-1} to 9.4×10^{-4} mol L^{-1}) invariable spectra indicate the predominance of π-stacking with the 0−0 transition being at 541 nm. The slight blue shift of about 8 nm compared to the spectrum in pure water indicates a somewhat more nonpolar environment for the aggregated PDI moieties. Upon further lowering the **PDC** concentration to 2.5×10^{-5} mol L^{-1} the proportion of a constant amount (i.e., the CMC) of nonaggregated **PDC**, supposedly in the open conformation, becomes more and more conspicuous by the emergence of its most intensive 0−0 transition at 531 nm (cp. Figure 4) which gradually superimposes the 0−0 transition of the π stacked **PDC** at 541 nm.

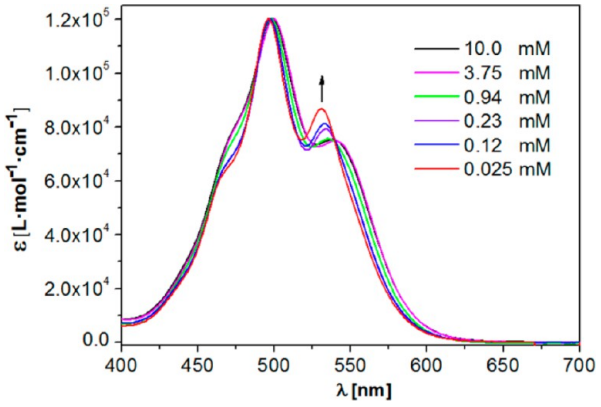

Figure 8. UV−vis dilution experiment of **PDC** directly dissolved in a binary water/THF mixture (30% THF). Concentration range: 10^{-2} mol L^{-1} to 2.5×10^{-5} mol L^{-1}.

Molecular Dynamics Simulations. Molecular modeling studies were used to determine factors that might explain the observed aggregation behavior of **PDC** in water. Atomistic molecular dynamics (MD) simulations (cp. Supporting Information section IV) in aqueous solution revealed the conformational flexibility of the monomer. Further US simulations provided insights into the equilibrium between the closed and the open conformations of **PDC**. As shown by the potential of mean force (PMF) in Figure 9, both conformations are likely to be present in solution. The quite low free-energy barrier of 13 kcal mol^{-1} between the conformations can be overcome at ambient temperature. The relative free energies of the two conformations indicate a preference of approximately 3 kcal mol^{-1} for the closed

DOI: 10.1021/ja512048t
J. Am. Chem. Soc. 2015, 137, 3308−3317

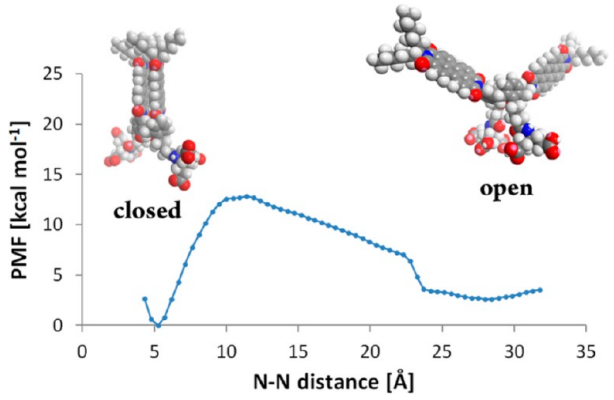

Figure 9. Potential of mean force (PMF) calculated for the transition between the closed and the open conformation of the **PDC** in water derived from an US trajectory. The graph displays the changes of the free energy (ΔG) against the increasing distance between the alkyl-substituted terminal nitrogen atoms of the perylene moieties during the conformational transition.

conformation in water. Thus, both conformations can play a role in the aggregation behavior shown in Figure 4.

Further MD simulations show that $\pi-\pi$ interactions between open conformers can lead to the formation of two types of arrangements (Figure 10A,B). These differ only with respect to the mutual orientation of the molecules. Angles between the perylenes (approximately 30° and 24°) and the interperylene distance (3.4 and 3.5 Å) for the trans- (Figure 10A) and cis-arrangements (Figure 10B), respectively, are very close and in good agreement with theoretical data of interacting perylene diimides.[34] In particular the transoidal interaction pattern (Figure 10A) suggests that ribbons from zigzag arranged oligomers can be formed easily. These may serve as precursors for larger assemblies.

The very low concentration of 10^{-7} mol L^{-1}, at which primarily π-stacked perylene moieties occur, however, indicates that intramolecular stacking of closed conformers dominates. However, interactions of open conformers would require a substantial deviation from an ideal cofacial arrangement of the interacting perylenes (Figure 10A,B). According to Spano et al.[25] the lack of Davydov splitting (DS) as well as the strong coupling (879 cm^{-1}) between interacting PDI moieties which can be directly calculated from the intensity ratio of the first two vibronic peaks of the absorption spectrum (Supporting Information, Figure SI 15) using eq 16 from ref 25 indicates an almost perfect cofacial arrangement of the PDIs, which is possible only for the closed conformation of **PDC**. These indications suggest an alternative model based on interdigitated closed conformers of **PDC** (Figure 10C). As a rough estimate, the size of the electron-dense aromatic region, which contributes most of the contrast in the electron microscopic images, extends to approximately 1.6 nm (taking about 1.1 nm for the length of the perylene moiety and 0.5 nm for the height of the calixarene cage). This is obviously shorter than the thickness of the ribbons or the tubule's walls observed in pure water (1.8–2.5 nm). A typical bilayer arrangement, however, would exceed 33.2 nm (double the electron-dense aromatic region plus a few Å occupied by the alkyl chains). Thus, an interdigitated arrangement in which only the perylene moieties of alternating molecules overlap, placing their alkyl chains between the opposing calixarene cages (Figure 10B) is likely. This arrangement allows the hydrophobic perylene-moieties,

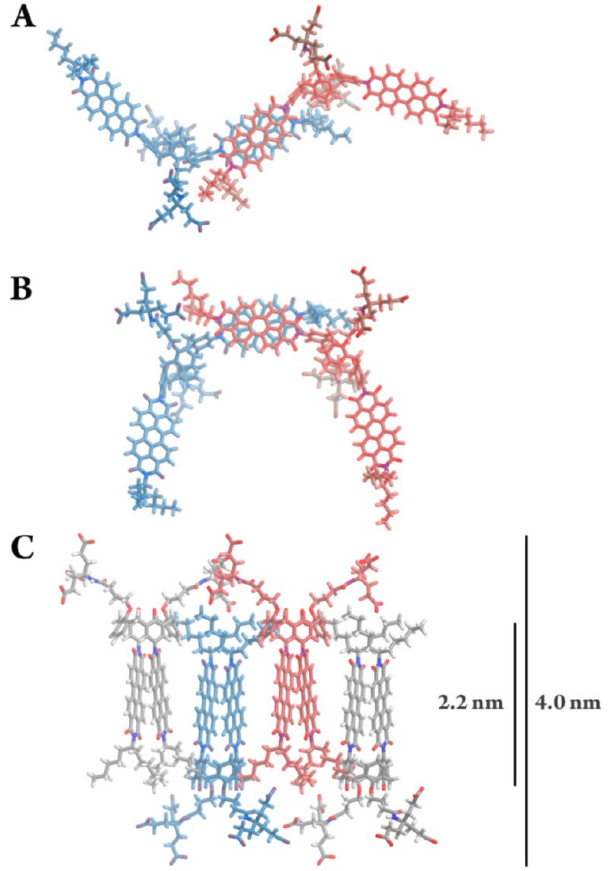

Figure 10. Possible arrangements of **PDC** in the aggregates formed in pure water. (A,B) Two types of interaction pattern of the open conformers are derived from molecular dynamic (MD) simulations. Especially the transoidal dimer (A) is suggestive of a band-like progression as a start of the ribbon-like aggregates. (C) An alternative arrangement can be deduced from π-stacked closed conformers. In such an interdigitated arrangement of the molecules, where the electron dense aromatic rings (i.e., the calixarene cages and the perylene moieties) reside in the core area, a better agreement with the density profiles of ribbons and tubes is obtained if compared to the arrangements in panels A and B, respectively.

alkyl chains, and calixarene cages, to be shielded from the aqueous solution by the hydrophilic dendritic head groups. The resulting dimension of the electron dense aromatic area of 2.2–2.3 nm agrees well with the cryo-TEM data.

The main difference between the two models is the role the $\pi-\pi$ interactions play in the assembling process: while the number of these interactions is increased during aggregation of open conformers, it does not change for closed conformers. Thus, in the latter case the self-assembly process is hydrophobically driven, whereas $\pi-\pi$ interactions contribute significantly in the first case. The observation of free perylene moieties in water by fluorescence spectroscopy is consistent with both an equilibrium between open and closed **PDC** molecules in solution (provided by MD) and the aggregation model based on the closed **PDC** (corroborated by the morphological peculiarities of the aggregates found by cryo-TEM). As long as aggregates are formed closed conformers are captured from the equilibrium. Upon dilution aggregation is reversed.

These models and calculations refer to pure aqueous samples. In water/THF mixtures, however, a completely

DOI: 10.1021/ja512048t
J. Am. Chem. Soc. 2015, 137, 3308–3317

different aggregation behavior is observed and a different arrangement of **PDC** must thus be assumed here. Although the density profile of fibrous assemblies suggests a tube-like organization (Supporting Information, Figure SI 18) geometrical considerations contradict this assumption. Tubes have to be constructed from bilayers of amphiphiles to expose hydrophilic surfaces both inward and outward. Considering the discovered dimensions, however, the curvature of the inner layer (~1−2 nm in diameter) would be too high to accommodate the large dendrons and the stiff calix[4]arene cages of **PDC**. Therefore, a rodlike arrangement seems to be more reasonable as a basis of the fibrous aggregates in water/THF (Figure 11). Such a rodlike arrangement of more or less

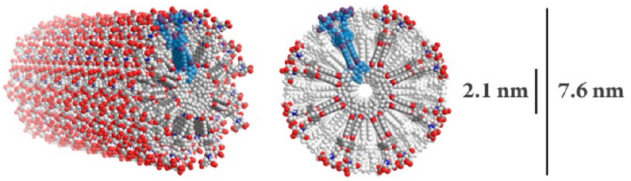

Figure 11. Perspective (left) and top view (right) of a proposed arrangement of the closed conformers of **PDC** leading to the fibrous aggregates that are observed in the binary water/THF mixtures. Dimensions of the model correspond to these fibrous aggregates. Obvious open spaces between the almost cylindrically shaped **PDC** molecules and in the core volume are thought to be filled with THF.

cylindrically shaped molecules would leave empty spaces within the hydrophobic areas of the aggregates. This deficit, however, can be compensated by the integration of THF molecules. This effect includes the interior hydrophobic volume of the rods and initiates a swelling process over time. This is supported by the finding that the size of the rod's inner hydrophobic part of aged samples (2.7 nm in diameter) clearly extends twice the length of the all-trans configured alkyl residues (~0.86 nm). Such kind of swelling of micellar aggregates has been observed earlier with dendron substituted calix[4]arene **1** in the presence of hexane.[9]

This model of THF-soaked **PDC** rods in water/THF not only explains our structural data from the cryo-TEM measurements and the spectral behavior of the samples but offers the clue to the question why the formation of rods obviously starts only after the addition of a critical amount of THF to the aqueous solutions. As stated above, the formation of fibrous assemblies can never be observed in aqueous solutions at low THF concentration (<5%). This seems to be reasonable in the light of the studies of Madhurima et al., who found that the formation of THF clathrates in water at low mole fractions ($0.03 \leq X_{THF} \leq 0.05$ and $0.07 \leq X_{THF} \leq 0.09$) can be monitored by the macroscopic behavior of the solution, that is, discontinuities in the course of changes of the contact angle.[35] Thus, competitive locking of THF in water clathrates may be responsible for the absence of rods in the binary mixtures with low THF content.

■ CONCLUSION

We have designed and synthesized a first representative of an amphiphilic perylene-calix[4]arene hybrid (**PDC**). In this architecture the hydrophilic dendritic head groups and the hydrophobic perylene moieties are oriented tetrahedrally in opposite directions. The compound is soluble in slightly basic water. UV−vis as well as fluorescence spectroscopy revealed H-type aggregation of the perylene diimide substituents over a large concentration range. The perylene and calixarene moieties facilitated detailed cryo-TEM studies in order to systematically explore the self-assembly behavior in water and in binary water/THF mixtures. **PDC** was found to form a variety of supramolecular assemblies with ribbon and tube-like structures. By adding THF to the water the aggregation behavior can be tuned to form a uniform population of fibrous aggregates with several hundred nanometers in length and 6.5−8.4 nm in diameter, which are swelling with time before **PDC** eventually precipitates from the solution. UV/vis or fluorescence spectroscopic data showed that these distinct structural changes do not affect the electronic properties of **PDC** and are thus only detectable by cryo-TEM studies. A very similar aggregation behavior of kinetically trapped, thermally stable aggregates in water which can be tuned into homogeneous assemblies by the addition of THF has just yet been published by Rybtchinski et al.[36]

Molecular dynamics simulation calculations showed that **PDC** can easily switch between an open tetrahedral conformation and a closed conformation with intramolecularly π-stacked perylene moieties. In water both conformations are stable and the equilibrium pathway between them is separated by only a small energy barrier. **PDC** represents a new lead structure of highly functional amphiphiles. The perylene building blocks serve both as structure/suprastructure determining units as well as reporter units for optical and cyro-TEM investigations. We are currently further exploiting the potential of this new class of tetrahedral amphiphiles by systematically varying the nature of the reporter dye and the hydrophilic dendron.

■ ASSOCIATED CONTENT

Supporting Information

Detailed synthetic, spectroscopic, microscopic, and MD calculation procedures, data of image analysis, and crystallographic data. This material is available free of charge via the Internet at http://pubs.acs.org.

■ AUTHOR INFORMATION

Corresponding Authors

andreas.hirsch@fau.de
christoph.boettcher@fzem.fu-berlin.de

Notes

The authors declare no competing financial interest.

■ ACKNOWLEDGMENTS

We are grateful to the Deutsche Forschungsgemeinschaft (DFG) for financial support.

■ REFERENCES

(1) Lehn, J.-M. *Science* **2002**, *295*, 2400.
(2) Whitesides, G. M.; Grzybowski, B. *Science* **2002**, *295*, 2418.
(3) (a) Martin, R. B. *Chem. Rev.* **1996**, *96*, 3043. (b) Israelachvili, J. N. *Intermolecular and Surface Forces*; 3rd ed.; Academic Press: Boston, MA, 2011.
(4) (a) Yan, Y.; Zhao, Y. S. *Chem. Soc. Rev.* **2014**, *43*, 4325. (b) Raghupathi, K. R.; Krishna, R.; Guo, J.; Munkhbat, O.; Rangadurai, P.; Thayumanavan, S. *Acc. Chem. Res.* **2014**, *47*, 2200. (c) Engberts, J.; Kevelam, J. *Curr. Opin. Collois Interface Sci.* **1996**, *1*, 779. (d) Rodler, F.; Linders, J.; Fenske, T.; Rehm, T.; Mayer, C.; Schmuck, C. *Angew. Chem., Int. Ed.* **2010**, *49*, 8747.

DOI: 10.1021/ja512048t
J. Am. Chem. Soc. 2015, 137, 3308−3317

(5) (a) Wei, A. *Chem. Commun.* **2006**, 1581. (b) Helttunen, K.; Shahgaldian, P. *New J. Chem.* **2010**, *34*, 2704. (c) Sansone, F.; Casnati, A. *Chem. Soc. Rev.* **2013**, *42*, 4623.
(6) Kellermann, M.; Bauer, W.; Hirsch, A.; Schade, B.; Ludwig, K.; Boettcher, C. *Angew. Chem., Int. Ed.* **2004**, *43*, 2959.
(7) Becherer, M.; Schade, B.; Boettcher, C.; Hirsch, A. *Chem.—Eur. J.* **2009**, *15*, 1637.
(8) Jäger, C. M.; Hirsch, A.; Schade, B.; Böttcher, C.; Clark, T. *Chem.—Eur. J.* **2009**, *15*, 8586.
(9) Jäger, C. M.; Hirsch, A.; Schade, B.; Ludwig, K.; Böttcher, C.; Clark, T. *Langmuir* **2010**, *26*, 10460.
(10) Wuerthner, F. *Chem. Commun.* **2004**, 1564.
(11) (a) Ford, W. E.; Kamat, P. V. *J. Phys. Chem.* **1987**, *91*, 6373. (b) Gvishi, R.; Reisfeld, R.; Burshtein, Z. *Chem. Phys. Lett.* **1993**, *213*, 338.
(12) (a) Kaiser, T. E.; Wang, H.; Stepanenko, V.; Wuerthner, F. *Angew. Chem., Int. Ed.* **2007**, *46*, 5541. (b) Schenning, A. P. H. J.; van Herrikhuyzen, J.; Jonkheijm, P.; Chen, Z.; Wuerthner, F.; Meijer, E. W. *J. Am. Chem. Soc.* **2002**, *124*, 10252. (c) Wuerthner, F.; Chen, Z.; Hoeben, F. J. M.; Osswald, P.; You, C.-C.; Jonkheijm, P.; von Herrikhuyzen, J.; Schenning, A. P. H. J.; van der Schoot, P. P. A. M.; Meijer, E. W.; Beckers, E. H. A.; Meskers, S. C. J.; Janssen, R. A. J. *J. Am. Chem. Soc.* **2004**, *126*, 10611.
(13) (a) Yagai, S.; Seki, T.; Karatsu, T.; Kitamura, A.; Wurthner, F. *Angew. Chem., Int. Ed.* **2008**, *47*, 3367. (b) Wu, H.; Xue, L.; Shi, Y.; Chen, Y.; Li, X. *Langmuir* **2011**, *27*, 3074. (c) Pochas, C. M.; Kistler, K. A.; Yamagata, H.; Matsika, S.; Spano, F. C. *J. Am. Chem. Soc.* **2013**, *135*, 3056.
(14) (a) Hippius, C.; Schlosser, F.; Vysotsky, M. O.; Boehmer, V.; Wuerthner, F. *J. Am. Chem. Soc.* **2006**, *128*, 3870. (b) Hippius, C.; van Stokkum, I. H. M.; Gsaenger, M.; Groeneveld, M. M.; Williams, R. M.; Wuerthner, F. *J. Phys. Chem. C* **2008**, *112*, 2476.
(15) Issac, A.; Hildner, R.; Ernst, D.; Hippius, C.; Wuerthner, F.; Koehler, J. *Phys. Chem. Chem. Phys.* **2012**, *14*, 10789.
(16) (a) Conner, M.; Janout, V.; Regen, S. L. *J. Am. Chem. Soc.* **1991**, *113*, 9670. (b) Scheerder, J.; Vreekamp, R. H.; Engbersen, J. F. J.; Verboom, W.; van Duynhoven, J. P. M.; Reinhoudt, D. N. *J. Org. Chem.* **1996**, *61*, 3476.
(17) Hippius, C.; van Stokkum, I. H. M.; Zangrando, E.; Williams, R. M.; Wykes, M.; Beljonne, D.; Wurthner, F. *J. Phys. Chem. C* **2008**, *112*, 14626.
(18) (a) Gutsche, C. D.; Iqbal, M. *Org. Synth.* **1990**, *68*, 234. (b) Gutsche, C. D.; Lin, L. G. *Tetrahedron* **1986**, *42*, 1633. (c) Gutsche, C. D.; Muthukrishnan, R. *J. Org. Chem.* **1978**, *43*, 4905.
(19) (a) Brettreich, M.; Hirsch, A. *Synlett* **1998**, 1396. (b) Newkome, G. R.; Behera, R. K.; Moorefield, C. N.; Baker, G. R. *J. Org. Chem.* **1991**, *56*, 7162. (c) Newkome, G. R.; Nayak, A.; Behera, R. K.; Moorefield, C. N.; Baker, G. R. *J. Org. Chem.* **1992**, *57*, 358.
(20) Kaiser, H.; Lindner, J.; Langhals, H. *Chem. Ber.* **1991**, *124*, 529.
(21) Case, D. A.; Darden, T. A.; T.E. Cheatham, I.; Simmerling, C. L.; Wang, J.; Duke, R. E.; Luo, R.; Walker, R. C.; Zhang, W.; Merz, K. M.; Roberts, B.; Hayik, S.; Roitberg, A.; Seabra, G.; Swails, J.; Götz, A. W.; Kolossváry, I.; Wong, K. F.; Paesani, F.; Vanicek, J.; Wolf, R. M.; Liu, J.; Wu, X.; Brozell, S. R.; Steinbrecher, T.; Gohlke, H.; Cai, Q.; Ye, X.; Wang, J.; Hsieh, M.-J.; Cui, G.; Roe, D. R.; Mathews, D. H.; Seetin, M. G.; Salomon-Ferrer, R.; Sagui, C.; Babin, V.; Luchko, T.; Gusarov, S.; Kovalenko, A.; Kollman, P. A.; *AMBER 12*; University of California: San Francisco, 2012.
(22) Wang, J. M.; Wolf, R. M.; Caldwell, J. W.; Kollman, P. A.; Case, D. A. *J. Comput. Chem.* **2004**, *25*, 1157.
(23) Bayly, C. I.; Cieplak, P.; Cornell, W. D.; Kollman, P. A. *J. Phys. Chem.* **1993**, *97*, 10269.
(24) (a) Kumar, S.; Bouzida, D.; Swendsen, R. H.; Kollman, P. A.; Rosenberg, J. M. *J. Comput. Chem.* **1992**, *13*, 1011. (b) Grossfield, A. Grossfield Laboratory. http://membrane.urmc.rochester.edu/ (accessed 2014).
(25) Kistler, K. A.; Pochas, C. M.; Yamagata, H.; Matsika, S.; Spano, F. C. *J. Phys. Chem. B* **2012**, *116*, 77.
(26) Sadrai, M.; Hadel, L.; Sauers, R. R.; Husain, S.; Krogh-Jespersen, K.; Westbrook, J. D.; Bird, G. R. *J. Phys. Chem.* **1992**, *96*, 7988.
(27) Hippius, C.; van Stokkum, I. H. M.; Zangrado, E.; Williams, R. M.; Wuerthner, F. *J. Phys. Chem. C* **2007**, *111*, 13988.
(28) Chen, Z.; Fimmel, B.; Wurthner, F. *Org. Biomol. Chem.* **2012**, *10*, 5845.
(29) Berlepsch, H. V.; Ludwig, K.; Schade, B.; Haag, R.; Bottcher, C. *Adv. Colloid Interface Sci.* **2014**, *208*, 279.
(30) Helfrich, W. *J. Chem. Phys.* **1986**, *85*, 1085.
(31) Yan, N.; Xu, Z.; Diehn, K. K.; Raghavan, S. R.; Fang, Y.; Weiss, R. G. *J. Am. Chem. Soc.* **2013**, *135*, 8989.
(32) Tidhar, Y.; Weissman, H.; Wolf, S. G.; Gulino, A.; Rybtchinski, B. *Chem.—Eur. J.* **2011**, *17*, 6068.
(33) Zhang, X.; Chen, Z.; Wurthner, F. *J. Am. Chem. Soc.* **2007**, *129*, 4886.
(34) (a) Fink, R. F.; Seibt, J.; Engel, V.; Renz, M.; Kaupp, M.; Lochbrunner, S.; Zhao, H. M.; Pfister, J.; Wurthner, F.; Engels, B. *J. Am. Chem. Soc.* **2008**, *130*, 12858. (b) Seibt, J.; Marquetand, P.; Engel, V.; Chen, Z.; Dehm, V.; Würthner, F. *Chem. Phys.* **2006**, *328*, 354.
(35) Purkayastha, D. D.; Madhurima, V. *J. Mol. Liq.* **2013**, *187*, 54.
(36) (a) Baram, J.; Weissman, H.; Tidhar, Y.; Pinkas, I.; Rybtchinski, B. *Angew. Chem. Int. Ed.* **2014**, *53*, 4123. (b) Baram, J.; Weissman, H.; Rybtchinski, B. *J. Phys. Chem. B* **2014**, *118*, 12068.

DOI: 10.1021/ja512048t
J. Am. Chem. Soc. 2015, 137, 3308−3317